Video Article

Helical Organization of Blood Coagulation Factor VIII on Lipid Nanotubes

Jaimy Miller*[1], Daniela Dalm*[1], Alexey Y. Koyfman[2,3], Kirill Grushin[1], Svetla Stoilova-McPhie[1,3]

[1]Department of Neuroscience and Cell Biology, University of Texas Medical Branch

[2]Department of Biochemistry and Molecular Biology, University of Texas Medical Branch

[3]Sealy Center for Structural Biology and Molecular Biophysics, University of Texas Medical Branch

*These authors contributed equally

Correspondence to: Svetla Stoilova-McPhie at svmcphie@utmb.edu

URL: http://www.jove.com/video/51254
DOI: doi:10.3791/51254

Keywords: Bioengineering, Issue 88, Cryo-electron microscopy, Lipid nanotubes, Helical assembly, Membrane-bound organization, Coagulation factor VIII

Date Published: 6/3/2014

Citation: Miller, J., Dalm, D., Koyfman, A.Y., Grushin, K., Stoilova-McPhie, S. Helical Organization of Blood Coagulation Factor VIII on Lipid Nanotubes. *J. Vis. Exp.* (88), e51254, doi:10.3791/51254 (2014).

Abstract

Cryo-electron microscopy (Cryo-EM)[1] is a powerful approach to investigate the functional structure of proteins and complexes in a hydrated state and membrane environment[2].

Coagulation Factor VIII (FVIII)[3] is a multi-domain blood plasma glycoprotein. Defect or deficiency of FVIII is the cause for Hemophilia type A - a severe bleeding disorder. Upon proteolytic activation, FVIII binds to the serine protease Factor IXa on the negatively charged platelet membrane, which is critical for normal blood clotting[4]. Despite the pivotal role FVIII plays in coagulation, structural information for its membrane-bound state is incomplete[5]. Recombinant FVIII concentrate is the most effective drug against Hemophilia type A and commercially available FVIII can be expressed as human or porcine, both forming functional complexes with human Factor IXa[6,7].

In this study we present a combination of Cryo-electron microscopy (Cryo-EM), lipid nanotechnology and structure analysis applied to resolve the membrane-bound structure of two highly homologous FVIII forms: human and porcine. The methodology developed in our laboratory to helically organize the two functional recombinant FVIII forms on negatively charged lipid nanotubes (LNT) is described. The representative results demonstrate that our approach is sufficiently sensitive to define the differences in the helical organization between the two highly homologous in sequence (86% sequence identity) proteins. Detailed protocols for the helical organization, Cryo-EM and electron tomography (ET) data acquisition are given. The two-dimensional (2D) and three-dimensional (3D) structure analysis applied to obtain the 3D reconstructions of human and porcine FVIII-LNT is discussed. The presented human and porcine FVIII-LNT structures show the potential of the proposed methodology to calculate the functional, membrane-bound organization of blood coagulation Factor VIII at high resolution.

Video Link

The video component of this article can be found at http://www.jove.com/video/51254/

Introduction

Blood coagulation Factor VIII (FVIII) is a large glycoprotein of 2,332 amino acids organized in six domains: A1-A2-B-A3-C1-C2 [3]. Upon Thrombin activation FVIII acts as the cofactor to Factor IXa within the membrane-bound Tenase complex. Binding of activated FVIII (FVIIIa) to FIXa in a membrane-depending manner enhances FIXa proteolytic efficiency more than 10^5 times, which is critical for efficient blood coagulation[4]. Despite the important role FVIII plays in coagulation and the Tenase complex formation, the functional membrane-bound FVIII structure is yet to be resolved.

To address this, single lipid bilayer nanotubes (LNT) rich in phosphatidylserine (PS), capable of binding FVIII with high affinity[8,9] and resembling the activated platelet surface have been developed[10]. Consecutive helical organization of FVIII bound to LNT has been proven to be effective for structure determination of FVIII membrane-bound state by Cryo-EM[5]. Functionalized LNT are an ideal system to study protein-protein and protein-membrane interactions of helically organized membrane-associated proteins by Cryo-EM[11,12]. Cryo-EM has the advantage over traditional structural methods such as X-ray crystallography and NMR, as the specimen is preserved at closest to the physiological environment (buffer, membrane, pH), without additives and isotopes. In the case of FVIII, studying the membrane-bound structure with this technique is even more physiologically relevant, as the LNT resemble closely by size, shape and composition the pseudopodia of the activated platelets where the Tenase complexes assemble *in vivo*.

Defects and deficiency of FVIII cause Hemophilia A, a severe bleeding disorder affecting 1 in 5,000 males of the human population[4,6]. The most effective therapy for Hemophilia A is life-long administration of recombinant human FVIII (hFVIII). A significant complication of the recombinant FVIII Hemophilia A therapy is the development of inhibitory antibodies to the human form affecting approximately 30% of Hemophilia A patients[13]. In this case, porcine FVIII (pFVIII) concentrate is used, as porcine FVIII displays low cross-reactivity with inhibitory antibodies against

human FVIII and forms functional complexes with human FIXa[7]. Establishing the membrane-bound organization of both porcine and human FVIII forms is important to understand the structural basis of FVIII cofactor function and implications for blood hemostasis.

In this study, we describe a combination of lipid nanotechnology, Cryo-EM, and structure analysis designed to resolve the membrane-bound organization of two highly homologous FVIII forms. The presented Cryo-EM data and 3D structures for helically organized porcine and human FVIII on negatively charged LNT show the potential of the proposed nanotechnology as basis for structure determination of FVIII and membrane-bound coagulation factors and complexes in a physiological membrane environment.

Protocol

1. Sample Preparation

1. Buffer exchange human FVIII-BDD[14] and porcine FVIII-BDD[15] against HBS-Ca buffer (20 mM HEPES, 150 mM NaCl, 5 mM $CaCl_2$, pH = 7.4) and concentrate to 1.2 mg/ml. Keep the protein solution at -80 °C.
2. Prepare lipid nanotubes (LNT) by mixing GalactosylCeramide (GC) and phosphatidylserine (PS) at 1:4 w/w ratio in chloroform. Evaporate the chloroform under argon and solubilize the lipids in HBS buffer to 1 mg/ml. Keep the LNT solution at 4 °C.

2. Cryo-electron Microscopy of FVIII-LNT

1. Cryo-EM Sample Preparation
    1. Glow discharge the 300 mesh Quantifoil R2/2 copper grids (carbon side up) in a mixture of O_2 and H_2 gas for 10 sec at 50 W.
    2. Mix the FVIII and LNT solutions in HBS-Ca buffer at 1:1 w/w ratio and incubate for 15 min at room temperature.
    3. Apply a drop of 2.5 µl of FVIII-LNT sample to the hydrophilic electron microscopy grid in the Vitrobot Mark IV humidified chamber (100% humidity).
    4. Blot and flash freeze the grid (one blot for 3.5 sec, blot force 1) in liquid C_2H_6, cooled down by liquid N_2 to obtain amorphous ice.
    5. Store grids in storage boxes under liquid N_2 (LN2).

2. Cryo-EM Data Collection
    NOTE: The JEM2100-LaB6 (year 2010) is equipped with a TEMCON operating system consisting of a computer connected to the electron microscope, a screen with windows reading the vacuum system, illumination system, HT, lens currents and so-on, and two panels: LEFT and RIGHT, placed on both side of the column. The beam shift X,Y knobs (SHIFT Y, SIFT Y) and the multifunction (DEF/STIG) knobs are on both panels. On the LEFT panel is the illumination (BRIGTHNESS) knob. On the RIGHT panel are: the magnification (MAG/CAM LENGTH) and focus (FOCUS) knobs and the three imaging (MAG1, MAG2, LOWMAG) and a diffraction (DIFF) modes buttons. We acquire our data in MAG1 at alpha 2. The minimum dose illumination conditions (MDS) required for Cryo-EM data acquisition are set with F1 through F6 buttons, top row on RIGHT panel. In this protocol the generic settings are used: F1 - raise/lower screen, F2 - SEARCH mode, F3 – FOCUS mode, F4 – PHOTO mode, F5 – MDS OFF/ON and F6 – BEAM BLANK, used to shield the specimen from radiation damage by deflecting the beam.
    1. Place the cryo-holder into the cryo-station and fill the Dewar of the holder and the cryo-station with LN2. When temperature reaches -192 °C, open shutter on the holder tip, place previously frozen Cryo-EM grid into the designated place and secure with a ring clamp.
    2. Insert the cryo-holder into the electron microscope. Refill the Dewar of the cryo-holder and the anti-contaminator chamber with LN2. Wait for the holder to stabilize for 30-60 min. Press F6 on and turn the filament on. When the filament is saturated, press F6 off and open shutter on holder to view the grid.
    3. Press Low Mag/alpha 1 (set at 200X mag) and locate areas with thin ice on the grid.
    4. Switch to MAG 1/alpha 2 to set minimum dose (MDS) mode and acquire Cryo-EM data at low electron doses, without damaging the specimen.
        1. Press F2 to set search mode. Set magnification at 40,000x. Enlarge beam with BRIGTNESS knob to minimal electron dose ~ 0.04 $e^-/Å^2 \cdot s$. Press DIFF to switch to diffraction mode. Set camera length to 120 cm with MAG/CAM LENGHT knob. Locate areas on the grid within the pre-selected areas in LOWMAG that have lipid nanotubes in the holes of the carbon film.
        2. Press F4 to set Photo mode at 40,000X magnification and set illumination with BRIGHTNESS knob at doses of 16-25 $e^-/Å^2 \cdot s$. Press Standard Focus button to set focus conditions adjusting the Z-height of the specimen with the Z UP/DOWN buttons (RIGHT control panel). Set defocus between -1.5 and -2.5 µm.
        3. Align SEARCH and PHOTO mode by drawing a square in the LIVE VIEW window on the digital camera monitor in SEARCH mode corresponding to the area to be imaged in PHOTO mode.
        4. Press F3 to set Focus mode at 100,000X magnification. Focus illumination to cover the CCD chip (~4 - 5 cm radius) and off axis to not irradiate the area to be imaged in PHOTO mode. Adjust defocus to ~ -1.5 and -2.5 µm with the FOCUS knob and correct for astigmatism of the image with DEF/STIG knobs.
    5. Select the FVIII-LNT to be imaged in SEARCH mode by acquiring live images in the LIVE VIEW window on the digital camera monitor. Center the FVIII-LNT in the square drawn on the LIVE VIEW window.
    6. Record a digital image on the CCD camera at 52,000X effective magnification and 0.5 sec exposure by switching to Photo mode and clicking the ACQUIRE button on the digital micrograph camera monitor. The image acquisition conditions are set such as the beam blank (SHUTTERS) open only when the image is acquired in PHOTO mode.
    7. Check the quality and defocus of the acquired image by pressing CTRL-F to obtain a Fast Fourier Transform (FFT).

3. 3D Reconstruction

NOTE: The image analysis software used for the 2D and 3D analysis: EMAN2 and IHRSR are freely available. EMAN2 can be downloaded from http://blake.bcm.edu/emanwiki/EMAN2/Install. The IHRSR software can be obtained from Professor Egelman: egelman@virginia.edu. The final

IHRSR refinements are run on the Texas advanced computing center cluster: http://www.tacc.utexas.edu/ at the University of Texas, Austin. The 3D reconstruction algorithm shown on **Figure 1** consists of two main steps: First selecting a homogenous set of helical segments (particles) with the 2D reference free alignment (RFA) algorithms implemented in EMAN 2, second achieving a 3D reconstruction based on the helical parameters and back projection algorithms incorporated in IHRSR. The first step utilizes the programs developed for selecting homogenous particle sets for 3D reconstruction with Single Particle SPA (algorithms) for which EMAN2 has been specifically developed and distributed: http://blake.bcm.edu/emanwiki/EMAN2. This step has been adapted to the Cryo-EM data. The second step is achieved with the IHRSR algorithm, which is specifically designed for the type of helical assemblies obtained with the recombinant Factor VIII forms. This algorithm has been documented extensively through the scientific literature[12].

1. Perform 2D image analysis with the EMAN2 scientific image-processing suite: http://blake.bcm.edu/eman2/doxygen_html[16] to select homogenous particle (helical segment) sets for helical reconstruction.
    1. Select Cryo-EM micrographs with straight and well-organized helical tubes with the digital camera software and visualization tools.
    2. Invert, normalize and filter for X-ray pixels in the *e2workflow.py* GUI, single particle reconstruction (spr) option: http://blake.bcm.edu/emanwiki/EMAN2/Programs/e2projectmanager
    3. Import the inverted, normalized and X-ray pixel filtered images in the *e2helixboxer.py* GUI. Select FVIII-LNT helical tubes and segment at 256 x 256 pixels (2.9 Å/pix) with 90% overlap using: http://blake.bcm.edu/emanwiki/EMAN2/Programs/e2helixboxer
    4. Evaluate the defocus from the original micrographs and apply contrast transfer function (CTF) correction (only phase correction) to the helical segments from the same micrographs with the *e2ctf.py* option incorporated in the *e2workflow.py*: http://blake.bcm.edu/emanwiki/EMAN2/Programs/e2ctf.
    5. Generate initial particles (helical segments) sets in the e2workflow.py GUI - SPR option: http://blake.bcm.edu/emanwiki/EMAN2/Programs/e2workflow.
    6. Calculate 2D class averages with the e2refine2d.py algorithm applying reference free k-mean classification to select homogenous data sets with the same diameter LNT and degree of helical order (**Figure 2**), following the script: 'e2refine2d.py --iter=8 --nalirefi=5 --nbasisfp=8 --path=r2d_001 --input=INPUT.hdf --ncls=51 --simcmp=dot --simalign=rotate_translate_flip --classaligncmp=dot --classraligncmp=phase --classiter=2 --classkeep=0.8 --classnormproc=normalize.edgemean --classaverager=mean --normproj –classkeepsig', changing the ncls value accordingly.
        1. Classify the initial data set in 150 classes 'ncls=151' over 8 iterations with 'classkeep=0.8', meaning that particles with less than 80% similarity to the class average are excluded from the given class. http://blake.bcm.edu/emanwiki/EMAN2/Programs/e2refine2d
        2. Merge particles from class averages with pronounced helical diffraction in *e2display.py* to create intermediate data set.
        3. Classify the intermediate data set in 50 classes 'ncls=51' to differentiate classes with same diameter and degree of order.
        4. Merge particles from classes with same diameter and degree of order in *e2display.py* to create the final data set for the three-dimensional reconstruction: http://blake.bcm.edu/emanwiki/EMAN2/Programs/emselector.

2. Perform helical reconstruction with the Iterative Helical Real Space Reconstruction (IHRSR) algorithm, as described in Egelman[17,18].
    1. Estimate the rise, Δz (Å) of the FVIII-LNT helix from the combined Fourier transform of the particles in the final data set.
    2. Define the azimuthal angle ΔΦ (º) by running parallel IHRSR refinements with a constant Δz, increasing ΔΦ from 5° to 60° in 5° increments.
    3. Run 100 consecutive IHRSR cycles for each final data set with a featureless cylinder as an initial volume and the initial helical parameters Δz and ΔΦ as defined in 3.2.1. and 3.2.2.
    4. Inspect the final volumes for convergence of the helical parameters and correspondence between class averages from the 2D classification of the final data set and the projections from the final IHRSR reconstruction.
    5. Impose symmetry to the final 3D reconstructions, corresponding to the asymmetric unit distribution observed in the final asymmetric 3D volumes: 4-fold for the human FVIII-LNT and 5-fold for the porcine FVIII-LNT. Run another 100 refinement cycles to generate a final symmetrized 3D reconstruction.
    6. Calculate the Fourier Shell Correlation curve for both volumes by first separating the corresponding data set in odd and even: 'e2proc2d.py <infile> <outfile> --split=2'. Then run 100 IHRSR consecutive refinements as described in 3.2.3. Calculate the FSC of the 3D volumes created from the odd and even datasets: 'e2proc3d.py evenvolume.mrc fsc.txt --calcfsc=oddmap.mrc'.

3. Visualize and Segment the FVIII-LNT volumes in UCSF chimera.
4. 1. Open the final volumes from step 3.2.5. in UCSF Chimera and set the contour level to 0.005 in the TOOLS > VOLUME DATA > VOLUME VIEWER option.
    2. In TOOLS > VOLUME DATA > SEGMENT MAP, select volume in SEGMENT MAP tab and click on SEGMENT to segment the volume.
    3. Group segments corresponding to one unit cell by selecting with CTRL+SHIFT and clicking group.
    4. Color the segments by unit cell and helix with ACTIONS > COLOR option to emphasize the structural features.

4. Electron Tomography

1. Negatively Stained FVIII-LNT Sample Preparation
    1. Prepare FVIII-LNT samples as for the Cryo-EM experiments.
    2. Glow discharges carbon-coated 300-mesh copper grid (carbon side up) in a mixture of O_2 and H_2 gas for 10 sec at 50 W as for Cryo-EM experiments.
    3. Apply a drop of 2.5 µl FVIII-LNT suspension with 6-nm colloidal gold nanoparticles to the grid, blot the excess liquid and negatively stain by applying 5 µl 1% uranyl acetate solution for 2 min. Blot the excess liquid and air dry the grid.

2. Electron Tomography Data Collection
    1. Transfer the grid into the single tilt holder.
    2. Transfer the holder in the electron microscope.

3. Collect tilt series automatically with the SerialEM software[19] at 2° increments over an angular range of -60° to +60° and record images with a CCD camera at 52,000X effective magnification, -6 to -10 µm defocus and electron dose of 150 - 170 electrons/Å^2·s per tomogram.

3. Electron Tomography Reconstruction of FVIII-LNT
Note: Reconstruct the pFVIII-LNT and hFVIII-LNT tilted series acquired in 4.2. with the ETomo option of the IMOD software following the tutorial: http://bio3d.colorado.edu/imod/doc/etomoTutorial.html
   1. Using a terminal window, open the tomogram in 3DMOD. http://bio3d.colorado.edu/imod/doc/3dmodguide.html.
   2. Bin the tomogram by 4 with the IMOD BINVOL command to decrease the size of the tomogram.
   3. Select the proper angle to rotate the lipid nanotube along the Y-axis in the binned tomogram using the IMOD ROTATEVOL command.
   4. Rotate the full tomogram with the IMOD ROTATEVOL command.
   5. Crop the selected lipid nanotube oriented along the Y-axis with the IMOD CLIP RESIZE command.
   6. Open the cropped sub-tomogram with 3DMOD.
   7. Click on the tomogram to visualize the arrangement of Factor VIII molecules along the slices in Z-axis and along Y-axis in the sub-tomogram volume.

Representative Results

Recombinant human and porcine FVIII were successfully organized helically on negatively charged single bilayer LNT, resembling the activated platelet surface**.** The helical organization of the human and porcine FVIII-LNT was consistent through the collected digital micrographs (**Figure 2)**. The control LNT and the human and porcine FVIII-LNT helical tubes were selected and segmented with the e2helixboxer.py GUI and initial data sets created with the e2workflow.py GUI, Single particle option (**Table 1**).

The helical order of the membrane-bound human and porcine FVIII-LNT was evaluated from the Fourier transform of the class averages with the e2display.py GUI (EMAN2) (**Figure 3**). The lipid bilayer in the best control LNT 2D class averages is well defined. The inner and outer leaflet and lower density of the membrane hydrophobic core are clearly visible (**Figure 3A**). The projected density of the membrane-bound human and porcine FVIII molecules oriented towards and perpendicular to the membrane surface is well defined and clearly shows the variations in the helical organization between the two proteins (**Figures 3B** and **3C**). The more pronounced twist for the human FVIII-LNT helical tubes indicates that the protein-protein interactions between adjacent membrane-bound FVIII molecules are consistently different for the two FVIII forms (**Figures 3B** and **3C**). Particles from class averages showing good helical organization (helical diffraction pattern) were merged in the *e2display.py* GUI to form an intermediate particle set (**Table 1**). The particles from the intermediate particle sets were again classified in 50 classes with the same constraints. The particles from class averages with the same diameter were merged in the final data sets (**Table 1**).

Initial 3D reconstructions for the human and porcine FVIII-LNT were carried out with 1,000 representative particles from the final human and porcine FVIII-LNT data sets. One hundred consecutive IHRSR iterations were run for each 3D reconstruction with a featureless cylinder (160 Å inner and 500 Å outer diameter), as initial volume. The axial rise (Δz) calculated from the combined Fourier transform of the helical segments (particles set) is equal to 41 Å for human FVIII-LNT and 36 Å for porcine FVIII-LNT (**Figures 4A** and **4B**). The initial azimuthal angle (ΔΦ) defined from the iterative search is estimated at 40.0° for the human FVIII-LNT and at 35.0° for the porcine FVIII-LNT. The final volumes are inspected for convergence of the helical parameters and correspondence between class averages and projections from the final reconstruction, also following the criteria described in[5]. The selected 3D reconstructions and corresponding helical parameters are imposed as initial volumes and initial helical parameters for a second IHRSR refinement of 100 cycles which converged to a four-start helical organization for the human FVIII-LNT with Δz = 41.1 Å and ΔΦ = 42.0° and a five-start helical organization for the porcine FVIII-LNT with Δz = 35.5 Å and ΔΦ = 34.8°. A final 100 IHRSR iterations imposing a 4-fold and a 5-fold helical symmetry for the human and porcine FVIII-LNT reconstructions respectively are carried out with initial volumes and corresponding helical parameters from the last asymmetric IHRSR refinements (**Figures 4C** and **4D**). The final volumes show 8 human FVIII and 10 porcine FVIII membrane-bound molecules organized around the helical axis (**Figure 5A)**. Each human FVIII molecule is translated 41.2 Å and rotated 42.0° from the previous one and each porcine FVIII molecule is translated 35.9 Å and rotated 35.2º from the previous one, corresponding to the helical parameters of the final 3D reconstructions (**Figure 5B**).

The reconstructed electron tomograms confirm the difference in the helical organization between the human and porcine FVIII-LNT obtained at the same experimental conditions. Comparison of the top views from the reconstructed tomograms and the 3D volumes from the helical reconstruction viewed in the direction perpendicular to the helical axis, further validates the correctness of the 3D reconstructions refined with the IHRSR helical parameters (**Figure 6**). The asymmetric 2D unit cell dimensions for the human FVIII-LNT 3D reconstruction are: a = 17.8 nm, b = 8.2, γ = 84° and for the porcine FVIII-LNT 3D reconstruction: a = 18.4, b = 7.2 and γ = 70° (**Figure 6**). The unit cell dimensions of human FVIII organized in membrane-bound 2D crystals are: a = 8.1, b = 7.0 and γ = 67º, which corresponds to the surface covered by one FVIII molecule viewed toward the membrane-surface[20]. Comparing the unit cell dimensions between FVIII organized in 2D and helical crystals indicates that both human and porcine FVIII molecules form dimers when helically organized on the LNT surface.

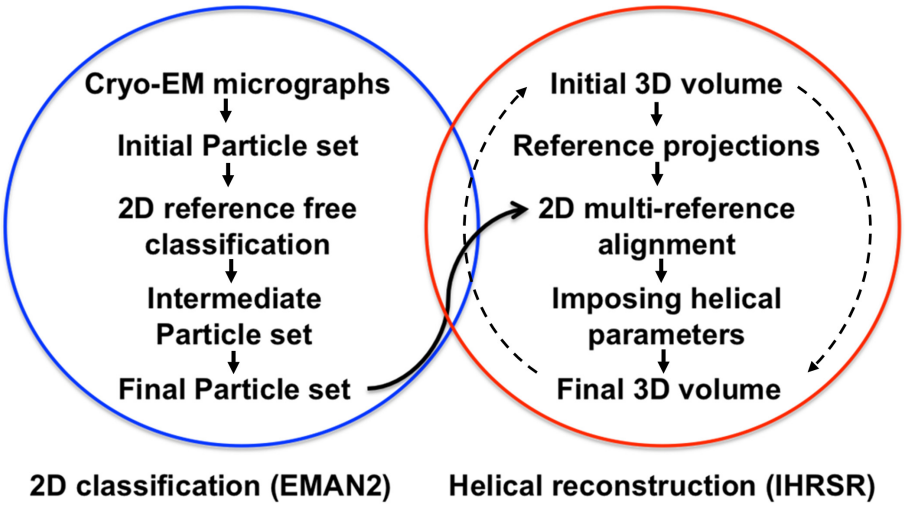

Figure 1. Structure analysis flow chart. The steps followed for the 2D classification analysis based on reference free alignment algorithms implemented in EMAN2[16] are circled in blue. The steps followed for the 3D analysis carried out with the iterative helical real space reconstruction algorithms (IHRSR) are circled in red. The iterative IHRSR cycles are denoted with dashed arrows.

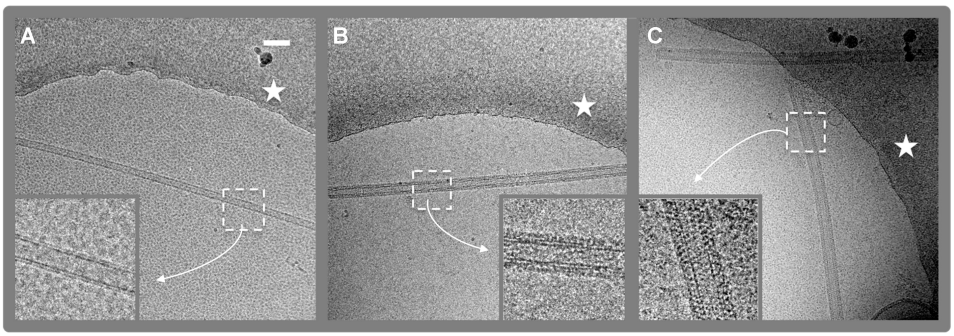

Figure 2. Cryo-EM digital micrographs. (4,096 x 4,096 pixels, 2.9 Å/pix) of lipid nanotubes (LNT) with and without bound FVIII. **A.** Control LNT. **B.** Human FVIII-LNT. **C.** Porcine FVIII-LNT. The edge of the hole in the carbon film in which the FVIII-LNT are suspended in amorphous ice is indicated with a white star. The protein and lipid densities are in black. The magnified views (insets) of 512 x 512 cropped areas (white dashed square) illustrate the difference in the helical organization of the human and porcine FVIII, respectively. The scale bar is 100 nm. Please click here to view a larger version of this figure.

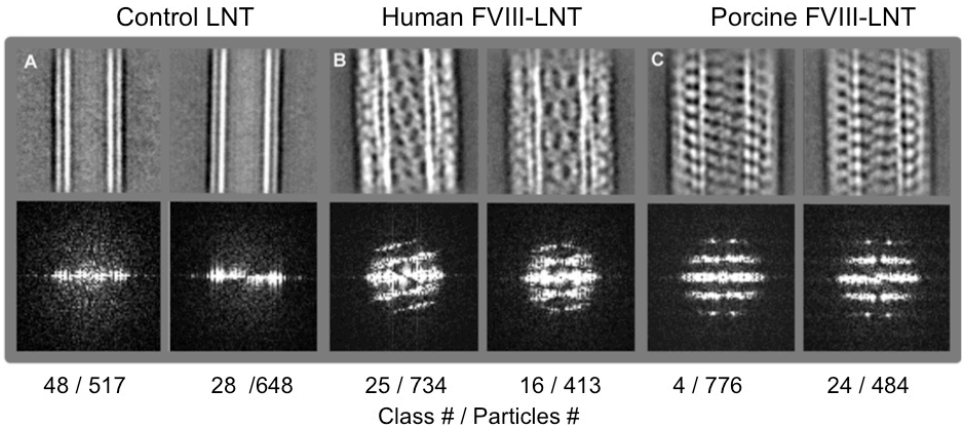

Figure 3. Representative 2D class averages (top row) and corresponding Fourier transforms (bottom row) from the intermediate particle sets (Table 1) classified in 50 classes. **A.** Control LNT **B.** Human FVIII-LNT **C.** Porcine FVIII-LNT. The class number and number of particles included in each class are indicated. The difference in helical order between the human and porcine FVIII is clearly seen on the images and confirmed by the diffraction patterns obtained from the Fourier transforms of these images. Please click here to view a larger version of this figure.

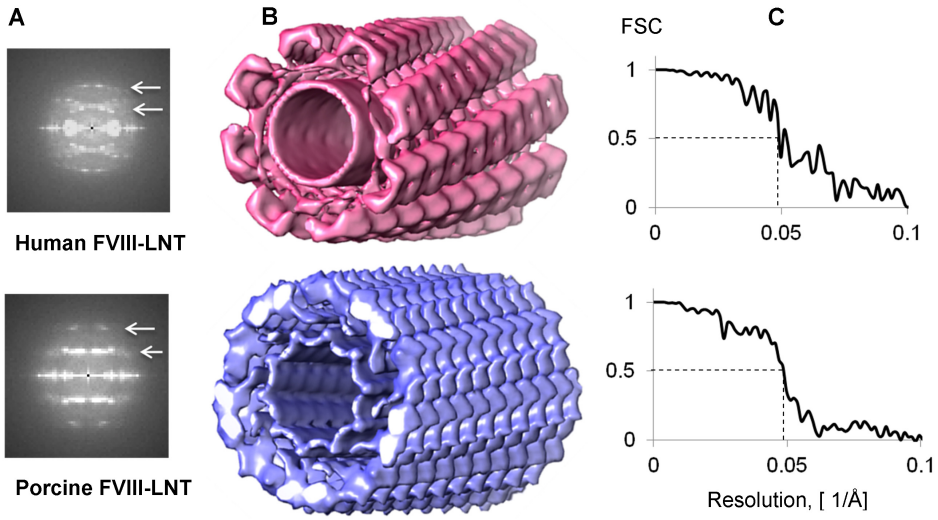

Figure 4. **3D helical reconstructions of human and porcine FVIII-LNT. A.** Combined Fourier transform from 1,000 helical segments. The first and second layer line are centered at 1/82 $Å^{-1}$ and 1/41 $Å^{-1}$ for human FVIII-LNT, and at 1/72 $Å^{-1}$ and 1/36 $Å^{-1}$ for porcine FVIII-LNT (white arrows). **B.** Surface representation of human in pink (Δz = 41.1 Å, $\Delta\Phi$ = 42.0º) and porcine in blue (Δz = 35.9 Å, $\Delta\Phi$ = 35.2º**)** FVIII-LNT 3D helical reconstructions. Both volumes are presented at 0.005 contour level (minimum density is 0 and maximum density 0.02, as calculated in UCSF Chimera, Volume viewer option[21]). The length of the FVIII-LNT tube is 256 pixels at 2.9 Å/pix. **C.** Fourier Shell Correlation (FSC) plots for human and porcine FVIII-LNT showing a resolution of 20.5 Å at FSC = 0.5.

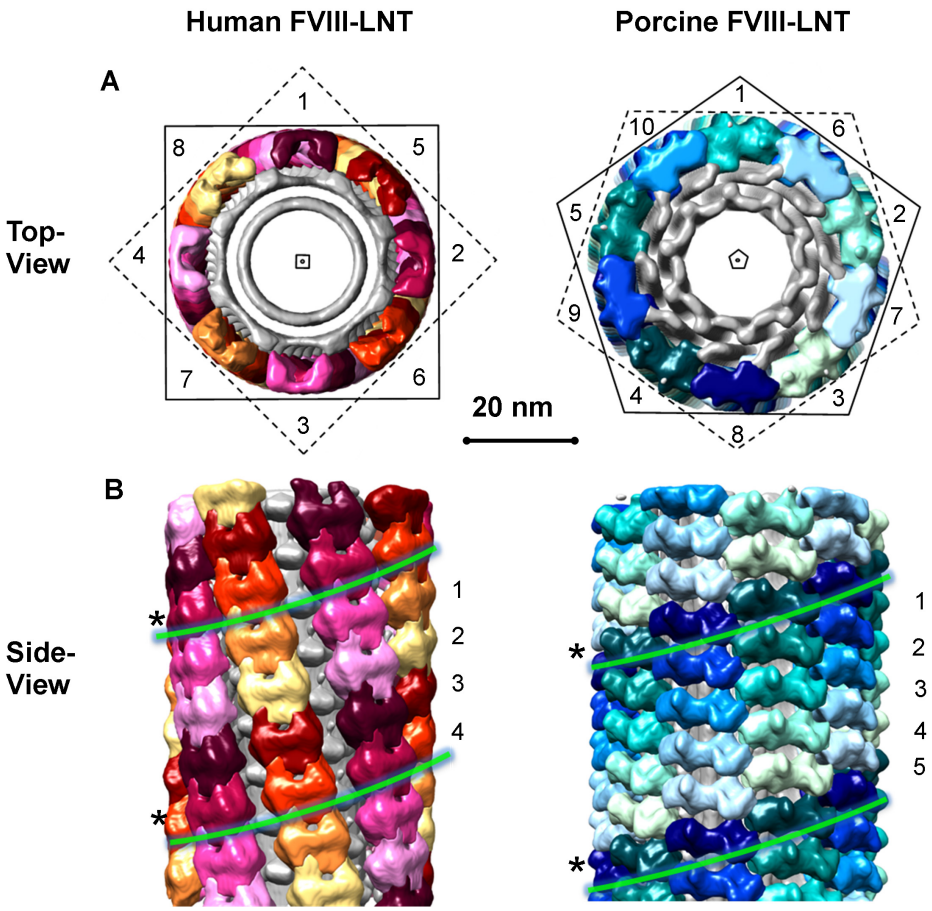

Figure 5. **Helical organization of human and porcine FVIII-LNT.** Segmented surface representation of human and porcine FVIII-LNT helical reconstructions, shown in **Figure 4B**. The volumes are segmented after imposing 4-fold symmetry to the human FVIII-LNT and 5-fold symmetry to the porcine FVIII-LNT. The asymmetric units are color coded yellow-red for the human FVIII-LNT and blue-green for the porcine FVIII-LNT. **A.** Views along the helical axis indicated with a square for the human and as a pentagon for the porcine FVIII-LNT. The human FVIII-LNT structure shows 8 molecules organized around the outer LNT membrane and the porcine FVIII structure shows 10 molecules organized around the outer LNT membrane, indicated with numbers. **B.** Views perpendicular to the helical axis. The human FVIII-LNT is a 4-start helical structure and the porcine FVIII-LNT is a 5-start helical structure. The individual one start helices are indicated with numbers and color-coded. We have emphasized one of the helices from each structure with a (*) and green lines. The scale bar is 20 nm.

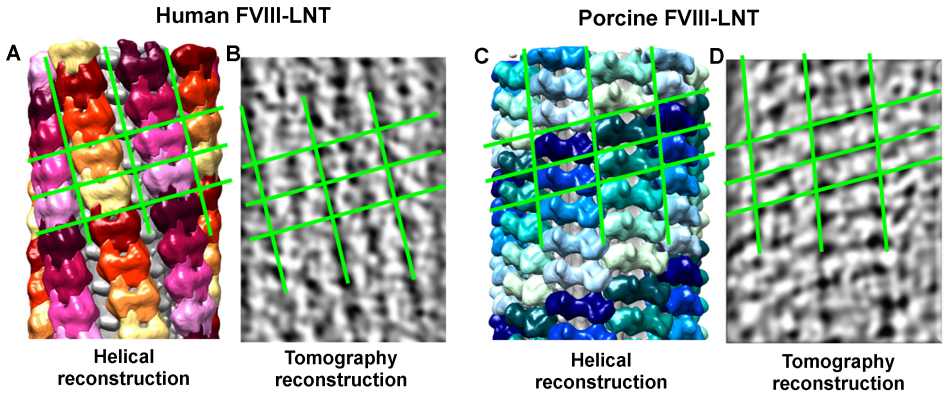

Figure 6. Comparison between the helical and tomography 3D reconstructions. The human FVIII-LNT (**A**) and porcine FVIII-LNT (**C**) helical 3D reconstructions are shown perpendicular to the helical axis. Each unit cell and individual helices are color-coded as in **Figure 5**. **B**. and **D**. are density representations of the 3D tomography reconstructions, viewed perpendicular to the helical axis. The 2D lattice reflecting the helical arrangement of the FVIII molecules is shown with green lines.

SAMPLES	cLNT	hFVIII-LNT	pFVIII-LNT
Initial Micrographs	61	474	542
Initial Particle sets	29113	60395	64665
Defocus (nm)	-4,051 ± 502	-3,643 ± 737	-3,443 ± 1,086
Intermediate Particle sets	25,907	27,305	22,773
Final Particle sets	25,907	10,455	10,430

Table 1. 2D analysis statistics following the algorithm presented in the flowchart on Figure 3.

Discussion

In this work a methodology is presented to differentiate between two membrane-bound organizations of highly homologous proteins: human and porcine FVIII self-assembled on lipid nanotubes in the conditions encountered in the human body.

In the described procedure, human and porcine FVIII are successfully organized helically on lipid nanotubes, which is the most critical step. The next critical step is to preserve the sample in thin amorphous ice by flash freezing at near liquid N_2 temperature. Preserving the sample in amorphous ice and LN2 temperature keeps the helical tubes hydrated and the protein-lipid macromolecular assemblies physiologically active. The final critical step is acquiring Cryo-EM data of sufficient quantity and quality for a high-resolution 3D structure at near LN2 temperature. Collecting data at near LN2 temperature further prevents dehydration of the sample in the high vacuum of the microscope and radiation damage from the electron beam.

To calculate the membrane-bound structure of the FVIII the first critical step is to obtain homogenous particles (helical segments) sets by applying 2D reference free classification and combine particles from classes with the same diameter and degree of order. The second critical step is to impose the right initial volume and helical parameters (rise and azimuthal angle) for the helical reconstruction. The third and final critical step is to validate the helical structure by comparing the 3D maps obtained by the helical and electron tomography (without imposed symmetry) reconstructions of the same specimen.

The presented methodology is unique in its capacity to resolve the functional structure of membrane-associated proteins at near physiological conditions. The LNT developed in our laboratory can be successfully used as a platform for helical organization of functional membrane-bound blood coagulation factors and achieve better resolution than for FVIII organized in membrane-bound 2D crystals and as single particles. Our goal is to further increase the resolution of our helical reconstructions by improving the homogeneity and quality of the final particle sets. Collecting more Cryo-EM micrographs at better Cryo-EM conditions (Field emission gun, energy filter, DE camera detectors) of FVIII-LNT helical filaments and therefore including larger initial particle sets for the 2D reconstruction will achieve this. Improving the FVIII-LNT helical assembly and 3D reconstruction algorithms will allow us to obtain sub-nanometer and near atomic resolution, which will unambiguously define the membrane-bound organization of this critical for blood coagulation protein.

Organizing helically homologous FVIII forms gives us also the opportunity to characterize how difference in sequence can correlate to differences in structure and function. Resolving the human and porcine FVIII membrane-bound structures by the methods described in this article can help identify the sequences, which when modified will improve the recombinant FVIII function. This knowledge will have significant clinical implications for drug discovery in both Thrombosis and Hemostasis fields.

Disclosures

The authors declare that they have no competing financial interest and they can be contacted directly regarding any of the procedures published in this manuscript.

Acknowledgements

This work is supported by a National Scientist Development grant from the American Heart Association: 10SDG3500034 and UTMB-NCB start up funds to SSM. The authors acknowledge the Cryo-EM and Scientific Computing facilities at the Sealy Center for Structural Biology at UTMB (www.scsb.utmb.edu), as well as Drs. Steve Ludtke and Ed Egelman for help with the 2D and 3D helical reconstruction algorithms.

References

1. Henderson, R. Realizing the potential of electron cryo-microscopy. *Quarterly Reviews of Biophysics.* **37**, 3-13, doi:doi:10.1017/S0033583504003920 (2004).
2. Fujiyoshi, Y., & Unwin, N. Electron crystallography of proteins in membranes. *Current opinion in structural biology.* **18**, 587-592, doi:10.1016/j.sbi.2008.07.005 (2008).
3. Toole, J. J. *et al.* Molecular cloning of a cDNA encoding human antihaemophilic factor. *Nature.* **312**, 342-347 (1984).
4. Fay, P. J. Factor VIII structure and function. *International journal of hematology.* **83**, 103-108, doi:10.1532/IJH97.05113 (2006).

5. Stoilova-McPhie, S., Lynch, G. C., Ludtke, S. J., & Pettitt, B. M. Domain organization of membrane-bound factor VIII. *Biopolymers.*, In Press, doi:10.1002/bip.22199 (2013).
6. Pipe, S. W. Hemophilia: new protein therapeutics. *Hematology / the Education Program of the American Society of Hematology. American Society of Hematology. Education Program.* **2010**, 203-209, doi:10.1182/asheducation-2010.1.203 (2010).
7. Gatti, L., & Mannucci, P. M. Use of porcine factor VIII in the management of seventeen patients with factor VIII antibodies. *Thrombosis and haemostasis.* **51**, 379-384 (1984).
8. Parmenter, C. D., Cane, M. C., Zhang, R., & Stoilova-McPhie, S. Cryo-electron microscopy of coagulation Factor VIII bound to lipid nanotubes. *Biochemical and biophysical research communications.* **366**, 288-293, doi:10.1016/j.bbrc.2007.11.072 (2008).
9. Parmenter, C. D., & Stoilova-McPhie, S. Binding of recombinant human coagulation factor VIII to lipid nanotubes. *FEBS letters.* **582**, 1657-1660, doi:10.1016/j.febslet.2008.04.018 (2008).
10. Wassermann, G. E., Olivera-Severo, D., Uberti, A. F., & Carlini, C. R. Helicobacter pylori urease activates blood platelets through a lipoxygenase-mediated pathway. *Journal of cellular and molecular medicine.* **14**, 2025-2034, doi:10.1111/j.1582-4934.2009.00901.x (2010).
11. Wilson-Kubalek, E. M., Chappie, J. S., & Arthur, C. P. Helical crystallization of soluble and membrane binding proteins. *Methods in enzymology.* **481**, 45-62, doi:10.1016/S0076-6879(10)81002-X (2010).
12. Egelman, E. H. Reconstruction of helical filaments and tubes. *Methods in enzymology.* **482**, 167-183, doi:10.1016/S0076-6879(10)82006-3 (2010).
13. Lusher, J. M. Development and introduction of recombinant factor VIII--a clinician's experience. *Haemophilia : the official journal of the World Federation of Hemophilia.* **18**, 483-486, doi:10.1111/j.1365-2516.2012.02804.x (2012).
14. Thim, L. *et al.* Purification and characterization of a new recombinant factor VIII (N8). *Haemophilia : the official journal of the World Federation of Hemophilia.* **16**, 349-359, doi:10.1111/j.1365-2516.2009.02135.x (2010).
15. Doering, C. B., Healey, J. F., Parker, E. T., Barrow, R. T., & Lollar, P. High level expression of recombinant porcine coagulation factor VIII. *The Journal of biological chemistry.* **277**, 38345-38349, doi:10.1074/jbc.M206959200 (2002).
16. Tang, G. *et al.* EMAN2: an extensible image processing suite for electron microscopy. *Journal of structural biology.* **157**, 38-46, doi:10.1016/j.jsb.2006.05.009 (2007).
17. Egelman, E. H. A robust algorithm for the reconstruction of helical filaments using single-particle methods. *Ultramicroscopy.* **85**, 225-234 (2000).
18. Egelman, E. H. The iterative helical real space reconstruction method: surmounting the problems posed by real polymers. *Journal of structural biology.* **157**, 83-94, doi:10.1016/j.jsb.2006.05.015 (2007).
19. Mastronarde, D. N. Automated electron microscope tomography using robust prediction of specimen movements. *Journal of structural biology.* **152**, 36-51 (2005).
20. Stoilova-McPhie, S., Villoutreix, B. O., Mertens, K., Kemball-Cook, G., & Holzenburg, A. 3-Dimensional structure of membrane-bound coagulation factor VIII: modeling of the factor VIII heterodimer within a 3-dimensional density map derived by electron crystallography. *Blood.* **99**, 1215-1223 (2002).
21. Goddard, T. D., Huang, C. C., & Ferrin, T. E. Visualizing density maps with UCSF Chimera. *Journal of structural biology.* **157**, 281-287, doi:10.1016/j.jsb.2006.06.010 (2007).

